Chapter 3

Plasma Proteome Profiling of Glioblastoma Multiforme using DNA-Encoded Antibody Microarrays: Characterizing Biomarker Signatures of Disease and Treatment Response

3.1 Introduction

Glioblastoma multiforme (GBM) [WHO grade IV astrocytoma] is the most common primary brain tumor in adults and the most aggressive form of glioma[1]. Due to its highly proliferative and infiltrative nature, GBM carries the poorest prognosis of any cancer, with a median patient survival of ~12 months, despite major advances in chemotherapy, radiation therapy, and surgery over the last few decades[2]. Although glioblastoma patients share many disease features in common, the fact that patients can differ tremendously in their response to therapy suggests that the cancer is molecularly heterogeneous. Indeed, it is known that genetically, there are two routes of glioblastoma development. Primary or de novo GBM, which is typically characterized by sudden onset

of high grade malignancy and an older age of onset, involves EGFR amplification and inactivation of the PTEN gene due to loss of heterogeneity at chromosome $10^{3,4}$. Secondary GBM, which is defined by progression from a lower-grade astrocytoma, and often presents at a younger age, initially involves chromosome 17 deletions and inactivation of the p53 gene, followed by a series of other mutations as the tumor undergoes malignant transformation[2-4]. However, even within these two broad categories, patients differ in the types of subsequent chromosomal alterations and mutations their tumors exhibit, as well as in rates of tumor growth and progression, overall survival, and types of treatments to which they respond.

Gene expression profiling has been instrumental in further elucidating key molecular players involved in GBM growth and progression, as well as the supporting cast of molecules that exhibit less pronounced changes[5,6], greatly facilitating the search for candidate GBM biomarkers. However, gene expression profiling provides a window only to RNA expression levels, whereas much of the information processing within the cell occurs at the level of protein network interactions. Often the relationship between RNA and protein expression level is nonlinear[7] due to additional transcriptional and post-transcriptional controls[8,9]. Therefore, key drug targets could be differentially expressed at the protein level but not the RNA level[10]. In addition, post-translational processing and modifications can alter the activities of proteins and their locations within the cell[8]. This information cannot be obtained solely by profiling gene expression.

Proteomic approaches pick up where genomic approaches leave off by allowing one to survey disease-related changes in global protein expression, find correlations between proteins that are similarly differentially expressed, and analyze those changes in

the context of known or prospective protein signaling pathways and networks. In particular, antibody-based microarray technology has facilitated the simultaneous high-affinity profiling of numerous proteins from relatively small samples of cell and tissue lysates, culture media[7], and bodily fluids, such as blood[11], urine[12], saliva, tears[13,14], and cerebrospinal fluid[15]. The advantages of this form of multiplexed protein detection over other approaches, such as 2D-PAGE and mass spectrometry, are its higher throughput and sensitivity, scalability, ease of use, cost-effectiveness, smaller sample requirements (< 50 µL), straightforward protein quantitation, and its ability to detect low abundance plasma proteins without the need for tedious protein fractionation steps[7,11,16]. As such, this technology represents a promising platform for novel disease-biomarker discovery. In addition, because small quantities of sample are sufficient to obtain enormous amounts of information, new opportunities are afforded for minimally-invasive diagnosis, stratification, and monitoring of cancer patients[16].

Blood is an ideal fluid for minimally-invasive detection of cancer-associated markers[17]. Cancer cells, like any other cell, secrete proteins into the bloodstream that can provide important information about their physiological and pathological state[17]. As well, intracellular proteins and cell-surface receptors are released into the circulation when cancer cells die. Antibody-based microarrays can permit the simultaneous, sensitive detection of many of these circulating factors from very small sample volumes – as little as a fingerprick's volume worth of blood (10 – 50 µL)[16]. It might nevertheless be expected that plasma detection of brain tumor markers would be challenging because the blood-brain barrier (BBB) greatly limits the free passage of proteins and other molecules between the two compartments[18]. However, the integrity of this barrier becomes greatly

compromised at sites of inflammation[19] or neovascularization[20-22], which both typically accompany glioblastoma tumors. In addition, glioblastoma tumors secrete soluble factors that disrupt the blood-brain barrier[23].

Unfortunately, for the vast majority of cancers and other diseases, no biomarkers have thus far been discovered with adequate specificity and sensitivity for whole-population screening or disease monitoring. Relatively few serum biomarkers have been FDA-approved for cancer monitoring, and just one – prostate specific antigen (PSA) – is approved for disease screening[24]. Likewise for glioblastoma, although gene expression profiling has allowed for the discovery of numerous protein biomarker candidates, none of these proteins on its own has achieved broad application for routine clinical diagnosis, prognosis, or monitoring of GBM, or for evaluating or predicting therapeutic response[25].

However, it has become increasingly recognized that large panels of proteins, in which each component protein has relatively poor disease specificity on its own, can, as a group, provide a highly sensitive and specific molecular signature of disease[26,27]. A number of studies have demonstrated the ability of antibody-based microarrays to identify protein expression patterns that can discriminate between patients with cancer (of the bladder[28], pancreas[29], prostate[30], or stomach[31]) and normal controls. In theory, a sufficiently informative protein biomarker panel could stratify a given disease into subgroups based on unique molecular phenotypes, much as has been shown in gene expression profile studies[5,10]. Treatments could then be customized to the tumor's specific set of molecular alterations. This would greatly contrast with the current expensive and time-consuming trial-and-error, watch-and-wait approach of administering a chemotherapeutic, awaiting a response, and then changing the medication if no

response is achieved. All the while, the patient's tumor continues to advance in grade and stage.

The routine use of antibody-based microarrays for multiplexed, high-throughput plasma biomarker detection and patient classification requires that these platforms be created using standardized methods that optimize sensitivity, reproducibility, cost, and compatibility with microfluidic chip based environments. While many approaches for arraying antibodies on slide surfaces have been investigated, DNA-directed antibody immobilization provides a number of unique advantages in this regard. For one thing, as compared to directly spotted antibodies, DNA-tethered antibodies exhibit less denaturation and possess greater orientational freedom, allowing a larger proportion of antibodies to be oriented such that their binding sites are accessible to cognate antigens[32,33]. Studies have also shown that this approach offers improved spot homogeneity and reproducibility, and far more economical use of antibody materials[32]. Importantly, for multiplexed point-of-care diagnostics, DNA-directed immobilization is amenable to microfluidic chip assembly because the antibodies can be arrayed subsequent to bonding of the PDMS stamp with the DNA-spotted slide – a thermal process that would otherwise destroy the antibodies[16,33].

The goal of the present study was to determine whether a plasma protein signature could be elucidated that would be able to differentiate patients with glioblastoma (n = 46) from healthy controls (n = 47) via a simple blood test that uses close to fingerprick volumes ($\leq$ 50 µL) of blood. We also sought to elucidate a plasma biomarker signature indicative of tumor growth – and, conversely, treatment response – in Avastin-treated GBM patients. Our platform consisted of capture-antibody arrays created by DNA-

directed assembly within ELISA-like wells. These antibodies were targeted against 35 distinct proteins known to be generally associated with tumor growth, survival, migration, invasion, angiogenesis, and immune-regulation. The platform allowed us to profile even low-abundance analytes (such as cytokines and growth factors) in plasma using microliter-scale sample volumes. We detected a number of proteins that were differentially expressed with high statistical significance ($p < 0.05$), allowing us to use these plasma biomarker signatures to classify patients into the aforementioned experimental and control groups with high sensitivity and specificity.

3.2 Materials and Methods

3.2.1 DNA-encoded antibody libraries (DEAL) technique

The antibody assembly platform used here is based on the DNA-encoded antibody library (DEAL) method, which has been reported elsewhere by our group[33]. When DEAL is utilized to measure proteins, it is used as follows (**Figure 3.5** in Appendix). Capture antibodies (CAs) against the protein of interest are chemically labeled with single-stranded DNA (ssDNA) oligomers, yielding ssDNA-CA conjugates. The coupling reaction is accomplished using succinimidyl 4-formylbenzoate (SFB, Solutink) and Succinimidyl 4-hydrazinonicotinate acetone hydrazone in *N,N*-dimethylformamide (DMF) (SANH, Solulink) as conjugation agents to link amine termini on DNA oligomers to the amine side-groups of proteins. A size-exclusion column is used to purify the product by removing excess unreacted DNA molecules. Separately, the complementary ssDNA oligomers (100 µM in a 50 % DMSO/water mixture) are

spotted onto a poly-L-lysine coated glass slide (150 µm spots spaced 300 µm center-to-center) using an array spotter (VersArray Chip Writer Pro, BioRad). Each spot also contains 10 µM of oligo **M** as a spot loading control. At the beginning of a DEAL protein assay, incubation of ssDNA-CA conjugates with the complementary spatially-patterned ssDNA array assembles the CAs onto those specific sites through DNA hybridization. This step transforms the DNA microarray into an antibody microarray that is ready for a protein sandwich assay. Biological samples (i.e. plasma isolated from human whole blood) can be applied onto the CA microarray and antigens can be captured. Finally, detection antibodies and/or fluorescent read-out probes are introduced sequentially to complete the immuno-sandwich assay. DNA oligomer sequences are chosen with appropriate melting temperatures to optimize 37 ^{o}C hybridization to complementary strands while minimizing cross-hybridization (< 5 % in fluorescence signal).

3.2.2 Antibody array platform

Our platform consists of ELISA-like wells assembled by bonding a PDMS slab with square holes to a poly-lysine coated glass substrate onto which 6 x 6 oligonucleotide arrays have been pre-spotted. Thirty-five distinct DNA-addressed antibodies are directed to their complementary spots during the assay. The assay wells accommodate up to 200 µL of sample, but in fact, only about 20 – 50 µL are needed to obtain a reasonable signal-to-noise. We used 50 µL of plasma for all of our assays.

3.2.3 Multiplexed assays on patient plasma

Each microarray well (12 wells/slide) was first blocked with 200 µL of blocking buffer – 3 % wt/vol bovine serum albumin fraction V (Sigma) in 150 mM 1x PBS

without calcium/magnesium salts (Irvine Scientific) – for 1 hour in a 37 $^{\circ}$C incubator. The wells were then aspirated, and 50 µL of a cocktail containing 35 different DNA-antibody conjugates (50 nM each) in blocking buffer were pipetted into the wells to transform the DNA arrays into capture-antibody arrays. After incubation at 37 $^{\circ}$C for 1 hour, the wells were aspirated, and then rinsed with blocking buffer 4 – 5 times to remove excess unbound conjugate. At this step, the wells were ready for the blood test. Fifty-microliter undiluted plasma samples were added to each well and allowed to incubate for 1 hour at 37 $^{\circ}$C. The samples were then aspirated and each well was again rinsed 4 – 5 times with blocking buffer. Next, a cocktail containing the 35 biotinylated detection antibodies (50 nM each) in blocking buffer was added to each well (50 µL) and was allowed to incubate for 1 hour at 37 $^{\circ}$C. The wells were aspirated and rinsed 4 – 5 times with blocking buffer, followed by incubation of a solution containing 50 nM Streptavidin-Cy5 (eBioscience) and 50 nM **M′**-Cy3 for 1 hour at 37 $^{\circ}$C. The wells were aspirated, and rinsed 4 – 5 times with blocking buffer. The PDMS well template was then peeled off the slide within a blocking buffer bath, and the slide was allowed to incubate in the bath for 1 minute at room temperature. The slide was then immersed in 150 mM 1x PBS, 1/2x PBS, and twice in deionized water in separate 50 mL falcon tubes for 1 minute, 10 seconds, and 2 seconds, respectively. The slide was then spun dry and scanned by a fluorescence microarray scanner.

3.2.4 Plasma collection and processing

Blood samples were collected by standard phlebotomy techniques in 10 mL blood collection tubes containing ACD-A anticoagulant (BD Vacutainer yellow-top glass tubes). The samples were centrifuged at *1500 x g* for 15 minutes, and the plasma was

collected and subdivided into 200 µL aliquots. Care was taken to ensure that plasma samples were frozen at -80 ^{o}C within 2 hours of collection to minimize degradation of plasma proteins by proteases. Each aliquot was thawed just once as needed.

3.2.5 Data processing and statistics

Post-assay, all array slides were scanned using a two-color laser fluorescence microarray scanner (GenePix 4200A Professional, Axon Instruments) at the same instrument settings – 70 % and 50 % for the laser power of the 635 nm and 532 nm channels, respectively. Optical gains were 550 and 500 for the 645 nm and 532 nm channels, respectively. Spot intensities were quantified with the software program GenePix Pro 6.0 using the fixed circle method. For each sample, the local background was subtracted from each spot, and the average and standard deviation were taken for each of the 35 sets of six repeated spots. A semi-global normalization method was used for chip-to-chip normalization. Briefly, the coefficient of variation (CV) was calculated for each analyte over all samples and ranked. The 15 % of analytes (5 analytes) with the lowest CV-values were used to calculate the normalization factor $N_i = S_i/\mu$, where S_i is the sum of the signal intensities of the 5 analytes for each sample, and μ is the average of S_i from all samples. The dataset generated from each sample was then divided by the normalization factor N_i. Universally, all datasets contained at least 4 analytes that had comparable intensities to negative controls run in separate experiments. Therefore, the net intra-assay intensities were calculated by subtracting each background-corrected analyte intensity by the mean intensity of the 4 lowest-intensity analytes. Unsupervised two-way average linkage hierarchical clustering (Cluster 3.0) was then performed on an entire patient cohort data set, and the resulting heatmap and dendrogram were viewed

using Java TreeView. The statistical significance (both Mann-Whitney and t-test *p*-values) of differential protein expression between experimental and control groups was analyzed using the *AnalyseIt* add-in for Microsoft Excel. This add-in was also used to generate box plots for each measured analyte across each study group.

3.2.6 Classification of patients

Two-by-two contingency tables and diagnostic parameters – sensitivity, specificity, negative predictive value (NPV), and positive predictive value (PPV) – were calculated by repeated random sub-sampling cross-validation. An Excel macro developed in-house was used to randomly assign 10 patients to a test set, leaving the remainder of patients as the training set. Unsupervised two-way average linkage hierarchical clustering (Cluster 3.0) was then performed on the entire patient cohort dataset (now containing 10 unknowns) and the resulting heatmap and dendrogram were viewed using Java TreeView. The ten unknown patients were then manually classified as belonging to the experimental (Group A) or control group (Group B) based on the following decision rules (x = fraction of members within the unknown's cluster that belong to same group):

1. The minimum number of clusters incorporating the unknown and at least 5 other members is analyzed. If all members of this cluster fall into the same group (x = 1), the unknown is classified as a member of that group with high confidence (this is considered a homogeneous zone). If x > 0.75, the unknown is still considered to be part of the majority group (with average confidence) but the cluster is no longer considered a homogeneous zone. If x < 0.75, then…

2. The minimum number of clusters incorporating the unknown and at least 8 other members is analyzed. If now $x > 0.75$, the unknown is considered to be part of the majority group. If $0.5 < x < 0.75$, the unknown is still considered to be part of the majority group, but with low confidence. In this case…

3. The minimum number of clusters incorporating the unknown and at least 14 other members is analyzed using the same decision rules as in 2.

4. If $x \sim 0.5$ after step 3, then the unknown remains unclassified and is removed from the analysis. Alternatively, an $x \sim 0.5$ is sufficient to remove the unknown sample from the analysis even if the unknown is grouped within a smaller cluster if the members of that cluster are closely correlated, yet far less correlated with the nearest neighboring cluster.

5. If in step 1, the unknown is part of a cluster containing 4 or fewer members that are all highly correlated with each other relative to the nearest neighboring cluster, the unknown is assigned to the majority group with low confidence if $0.5 < x < 0.66$, average confidence if $0.66 < x < 0.75$ and high confidence if $x = 1$.

6. If two or more unknowns are nearest neighbors, these unknowns remain unclassified and are removed from the analysis.

This random sub-sampling was then repeated 10 times with replacement (100 unknown events), such that some patients may have been randomly assigned to a test sample more than once, while others not at all. An Excel macro developed in-house then compared the predicted and actual classifications, and output the total number of true-positives, false-positives, true-negatives, and false-negatives in a 2 x 2 contingency table, as well as the sensitivity, specificity, NPV, and PPV of the diagnostic evaluation. This constituted the full diagnostic evaluation for a dataset. For the two patient cohorts examined in this study, diagnostic evaluation was also performed on trimmed datasets consisting of subsets of n proteins (from the initial 35-protein panel) that exhibited the most statistically significant differential expression between experimental and control groups (where n = 3, 6, 9, 12, 16, 20, 25). For each dataset, points were plotted in ROC space (sensitivity vs. 1 – specificity) to assess the predictive power of the test.

3.3 Results

3.3.1 Evaluation of DNA directed antibody microarrays

Preliminary experiments were run in advance to validate a set of 35 orthogonal oligos that exhibited minimal cross-hybridization ($< 5\%$). In addition, the full panel of DNA-conjugated antibodies was validated with a set of cognate recombinants to ensure that there was minimal cross-talk between each recombinant and non-cognate spots. Each DNA spot was loaded with reference DNA (10 %), which, once hybridized with a dye-conjugated complement, served as a DNA-loading control. For each oligo, the spot loading was highly consistent both across an entire slide as well as between slides.

Figure 3.1. Assay platform and methodology. Polylysine-coated slides were spotted with 36 distinct oligos in 6 x 6 array repeats. **i.** A PDMS slab containing square holes was set on top of the spotted substrates, forming ELISA-like assay wells. Assays were performed by **ii.** blocking the wells with BSA, **iii.** incubating with conjugates to transform the DNA microarray into an antibody microarray, **iv.** adding a different patient plasma sample to each well, **v.** incubating with biotinylated detection antibodies, **vi.** adding Streptavidin-Cy5 (Red Spots) and **M′**-Cy3 (Green Reference Spot), with rinses between steps. Each well contained six full repeats of the 6 x 6 antibody arrays. The platform was used to detect 35 distinct proteins from $40 - 50 \mu L$ of plasma. Readout was performed with a flourescence scanner.

The fluorescent readouts from all plasma samples assayed on the 35-plex antibody array platform were analyzed for spot homogeneity, reproducibility, and signal-to-noise. A representative image of the fluorescent readout from a single assay well is shown in **Figure 3.1**. Each well contained a total of six repeats of 6 x 6 spot arrays (35 antibodies + 1 green Cy3-conjugated reference oligonucleotide). The spots are circular, well-defined, and radially homogeneous. There was very little intra-assay variation in the

intensities of each set of 6 spot repeats. In addition, spot intensities tended to be highly consistent even between duplicate assays run on separate slides.

3.3.2 Classification of GBM patients versus healthy controls

We compared plasma samples from 46 GBM patients (72 samples: for some patients, plasma samples from multiple collection dates were available) with those of 47 healthy controls with respect to the plasma levels of 35 different proteins known to be generally associated with tumor growth, survival, invasion, migration, and immunoregulation. Two-way average-linkage hierarchical clustering allowed these two groups to be discriminated with a sensitivity and specificity of 84 ± 15 % and 89 ± 31 %, respectively (**Figure 3.2a**). The heat map is divided into numerous islands of GBM patient, healthy control, and mixed population clusters without a clean separation between the two groups. We then sought to determine whether the diagnostic accuracy could be improved by removing those test samples from diagnostic evaluation that did not fall into highly homogeneous clusters (i.e. > 70% of the cluster members belong to the same group). Within the subpopulation of test samples that fell into highly discriminatory clusters, the sensitivity and specificity improved to 90 ± 14 % and 94 ± 8 %, respectively, albeit with a diagnosable population size that was 70 % of the original. Among test samples that clustered entirely with members of a single group ("homogeneous zones"), the sensitivity and specificity both approached 100 %. Thirty percent of samples fell into one of these homogeneous zones, allowing that subpopulation to be diagnosed with near-perfect accuracy.

Figure 3.2a. GBM patients vs. healthy controls

Average linkage hierarchical clustering (unsupervised) was performed on 35-protein datasets from each of 72 GBM patient plasma samples and 47 Healthy Control samples. A computer program was used to randomly assign patients to trial and test sets (multiple times), and the tumor growth status of each test set member (unknown) was predicted based on the status of nearest neighbors in its cluster. 2x2 tables were generated and relevant statistical parameters calculated for diagnostic tests that evaluated: **i)** all unknowns on the heatmap; **ii)** unknowns in clusters where a sizeable majority of members -including the nearest neighbor - shared the same status; **iii)** unknowns in completely homogeneous clusters where *all* members shared the same status - so-called "homogeneous zones" (highlighted).

Figure 3.2b. GBM patients vs. healthy controls using the 9 proteins with the most statistically significant p-values. The heat map in Figure 3.2a was "trimmed" by performing average linkage hierarchical clustering (supervised) on the nine proteins that exhibited the most significant differences (lowest p-values) between GBM patients and healthy controls. Note the significant improvement in stratification of patients into just two main relatively homogenous groups – a "GBM patient" cluster and a "Healthy Control" cluster. Compare with the more numerous small clusters and "mixed" groups in Figure 3a. TP = True Positive, TN True Negative, FP = False Positive, FN = False Negative, PPV = Positive Predictive Value, NPV = Negative Predictive Value. Label Colors: Magenta – Growth; Green – No Growth; Blue – Growth Possible or Slow. High-lighted areas on Heat Map are "zones".

We then repeated the cluster analysis with a trimmed panel that included only the nine proteins with the most statistically significant (Mann-Whitney and t-test p-values < 0.05) differential expression (**Figure 3.2b**). These included: MMP3, PDGF, IP10, IGFBP2, VEGF, IL13, GM-CSF, MMP9, and CRP. The resultant heat map shows far improved classification of GBM patients and healthy controls into two separate clusters,
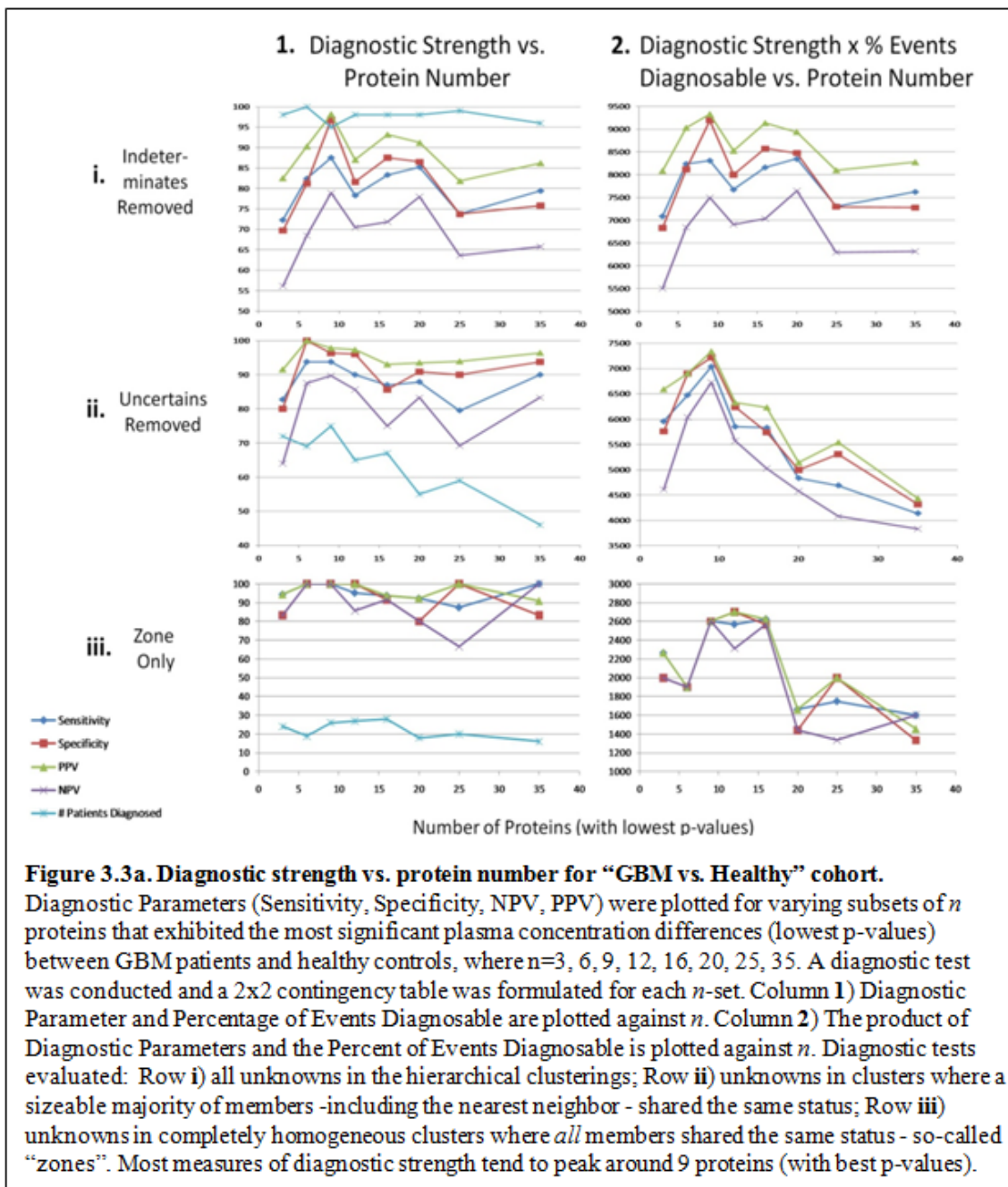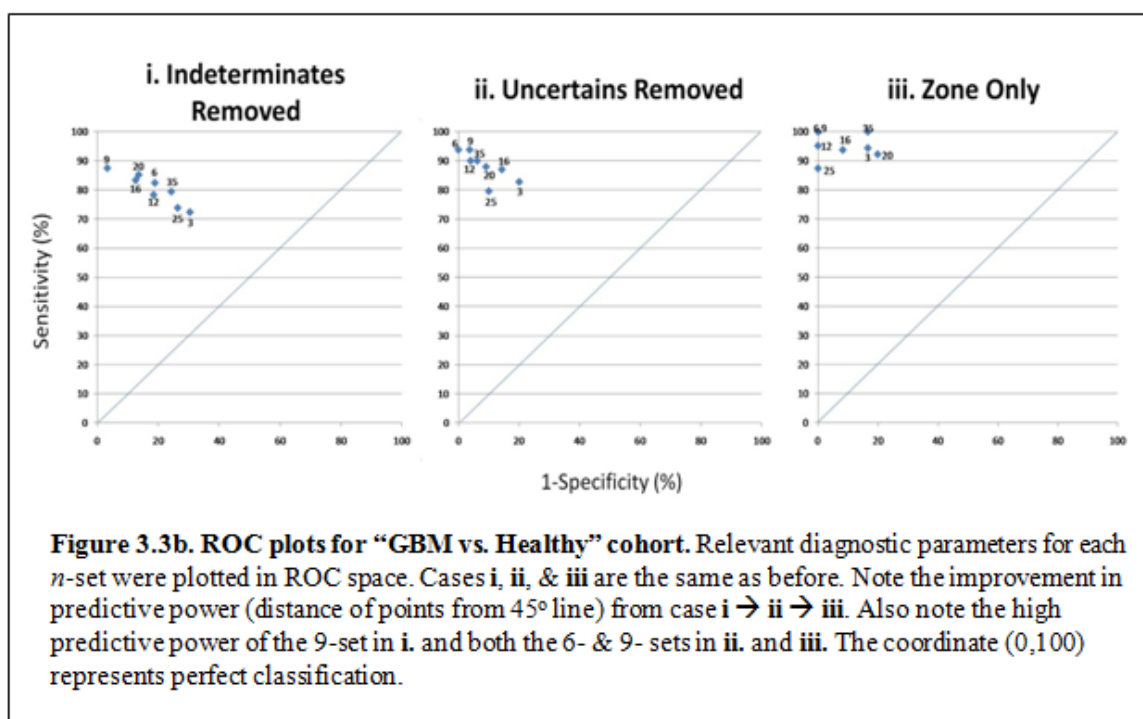
with few misclassifications in each cluster. By using this trimmed protein panel, the sensitivity and specificity achieved were 88 ± 13 % and 97 ± 8 %, respectively. As before, those samples (20 % of the sample population) that did not decisively cluster with a particular group were removed from diagnostic evaluation, and the sensitivity and specificity among the resulting diagnosable population improved to 94 ± 10 % and 96 ± 8 %, respectively. Again, both sensitivity and specificity approached 100 % among test samples that clustered within perfectly homogeneous zones.

3.3.3 Diagnostic strength as a function of protein panel size

The cluster analysis was repeated for n-protein subsets of the original 35 protein panel, where n = 3, 6, 9, 12, 16, 20, 25, & 35 of the most statistically significant discriminators of GBM and health status. Diagnostic test sensitivity, specificity, and positive and negative predictive values were calculated for each of these subsets. Those test samples that did not decisively cluster with a particular group were removed from the evaluation. As can be seen in **Figure 3.3a**, the sensitivity and specificity remain about level as one trims the panel from 35 to 20 proteins. Both parameters increase as the panel is trimmed from 16 proteins onwards, with a peak at 6 proteins, followed by a sharp drop as the panel size is reduced further. On the other hand, the percentage of samples evaluable increases steadily as one trims the panel from 35 proteins down to 9 proteins and then tapers off. Since the strength of a diagnostic test lies not only in its diagnostic accuracy but also in the percentage of the population it can evaluate, we designated an artificial parameter S to represent the product of a diagnostic value and the percentage of patients diagnosable for each n-protein subset. As can be seen in **Figure 3.3a**, this parameter increases steadily as the protein panel size is reduced, peaking at 9 proteins

and then falling off sharply. Therefore, the 9-protein subset appears to optimize test performance by achieving a high diagnostic accuracy while still maintaining the ability to diagnose a large fraction of the sample population.

Figure 3.3a. Diagnostic strength vs. protein number for "GBM vs. Healthy" cohort.
Diagnostic Parameters (Sensitivity, Specificity, NPV, PPV) were plotted for varying subsets of n proteins that exhibited the most significant plasma concentration differences (lowest p-values) between GBM patients and healthy controls, where n=3, 6, 9, 12, 16, 20, 25, 35. A diagnostic test was conducted and a 2x2 contingency table was formulated for each n-set. Column **1**) Diagnostic Parameter and Percentage of Events Diagnosable are plotted against n. Column **2**) The product of Diagnostic Parameters and the Percent of Events Diagnosable is plotted against n. Diagnostic tests evaluated: Row **i**) all unknowns in the hierarchical clusterings; Row **ii**) unknowns in clusters where a sizeable majority of members -including the nearest neighbor - shared the same status; Row **iii**) unknowns in completely homogeneous clusters where *all* members shared the same status - so-called "zones". Most measures of diagnostic strength tend to peak around 9 proteins (with best p-values).

Figure 3.3b. ROC plots for "GBM vs. Healthy" cohort. Relevant diagnostic parameters for each *n*-set were plotted in ROC space. Cases **i**, **ii**, & **iii** are the same as before. Note the improvement in predictive power (distance of points from 45° line) from case **i** → **ii** → **iii**. Also note the high predictive power of the 9-set in **i**. and both the 6- & 9- sets in **ii**. and **iii**. The coordinate (0,100) represents perfect classification.
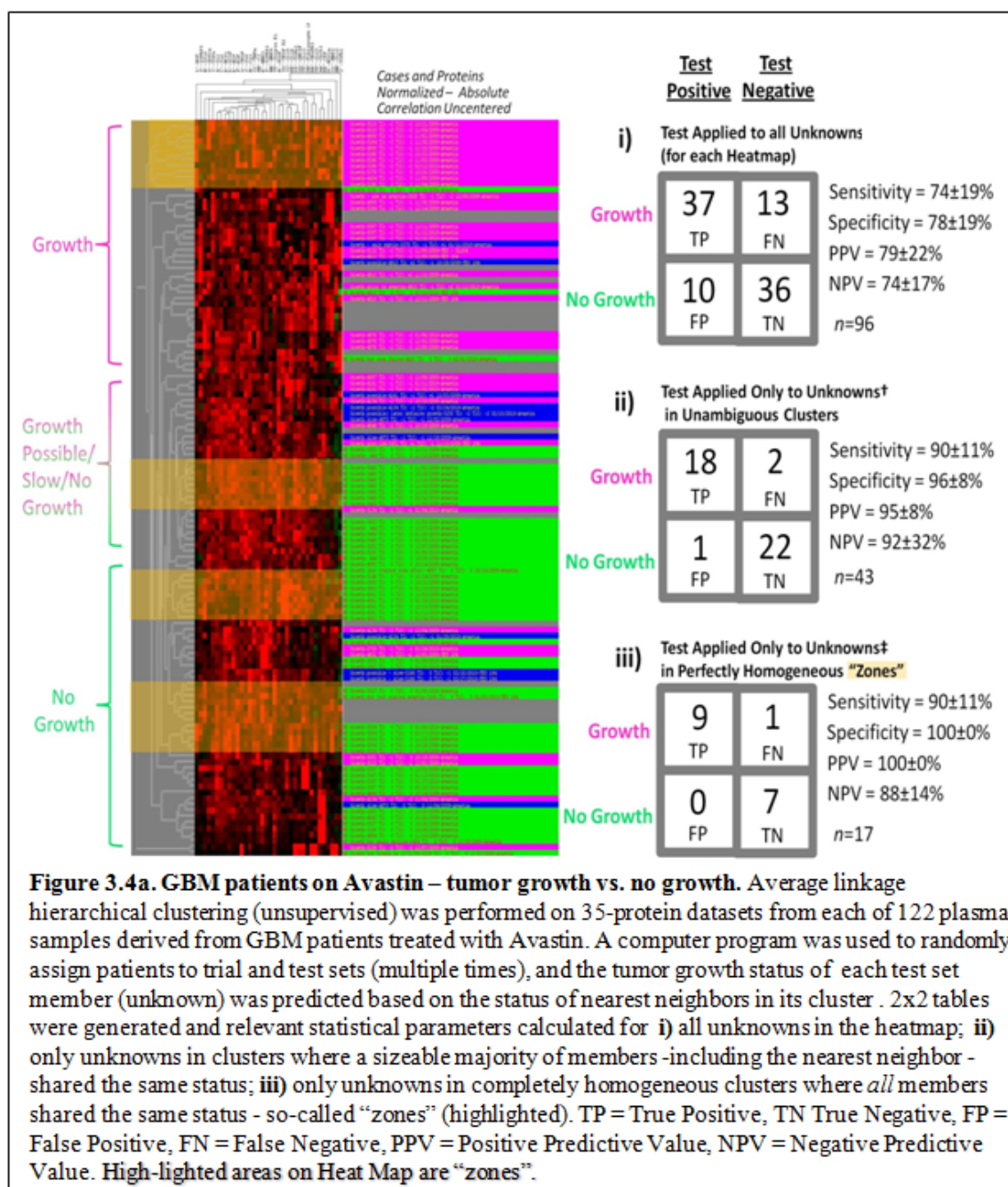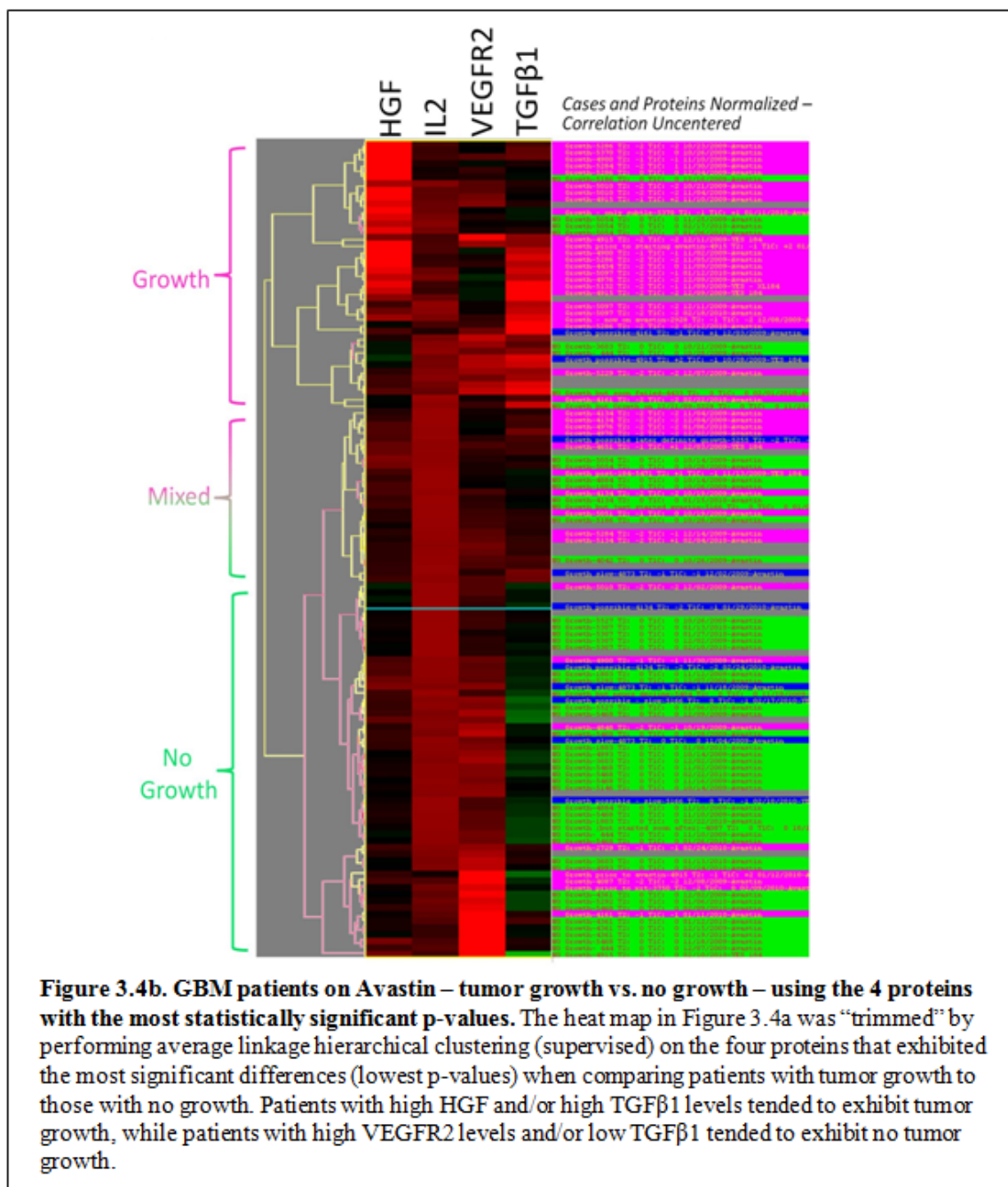
The predictive power of each *n*-protein subset for classifying GBM patients and healthy controls can also be evaluated by plotting the true positive rate (sensitivity) vs. the false positive rate (1 – specificity) for each subset. As observed in **Figure 3.3b**, the 6- and 9-protein subsets yield points in ROC (Receiver-Operating Characteristic) space that are farthest in perpendicular distance from the 45° line, suggesting that this number of differentially expressed proteins maximizes the predictive power. Points for all protein-panel subsets move farther from the diagonal line as the sample population is trimmed to include: only those samples in clusters that are highly biased – the great majority (> 70 %) of members belong to either the GBM patient or healthy control groups (as in **Figure 3.3b ii**); or, only those samples in clusters that are completely biased – all members belong to one of the two groups (as in **Figure 3.3b iii**). Perfect classification was achievable in both 6- and 9-protein subsets when analyzing only the subset of test samples that were located within perfectly homogeneous clusters. As a whole, the data in

Figure 3.3 shows that by performing cluster analysis on patient plasma samples assayed for the 6 or 9 proteins most significantly differentially expressed, a very high degree of predictive power could be achieved among samples in highly biased clusters. In addition, the 9-protein set optimized the predictive power and the number of patients diagnosable. Furthermore, a subgroup of these patients who fell into perfectly homogeneous clusters could be diagnosed with near certainty.

3.3.4 GBM patients on Avastin – classification of tumor growth vs. no growth

We then assayed plasma samples from GBM patients treated with the chemotherapeutic drug Avastin (Bevacizumab) with respect to the same 35-protein panel as before. Specifically, we compared 52 samples from 25 patients who exhibited tumor growth (according to MRI imaging) with 51 samples from 21 patients who exhibited no tumor growth since their last evaluation. Two-way average linkage hierarchical clustering allowed these two groups to be discriminated with a sensitivity and specificity of 74 ± 10 % and 78 ± 19 %, respectively (**Figure 3.4a**). When only patient samples within highly biased clusters were analyzed (45 % of the total sample population), the sensitivity and specificity improved to 90 ± 11 % and 96 ± 8 %, respectively. The sensitivity remained the same but the specificity increased to 100 % when test samples only in perfectly homogeneous clusters were analyzed (20 % of sample population).

Figure 3.4a. GBM patients on Avastin – tumor growth vs. no growth. Average linkage hierarchical clustering (unsupervised) was performed on 35-protein datasets from each of 122 plasma samples derived from GBM patients treated with Avastin. A computer program was used to randomly assign patients to trial and test sets (multiple times), and the tumor growth status of each test set member (unknown) was predicted based on the status of nearest neighbors in its cluster . 2x2 tables were generated and relevant statistical parameters calculated for **i)** all unknowns in the heatmap; **ii)** only unknowns in clusters where a sizeable majority of members -including the nearest neighbor - shared the same status; **iii)** only unknowns in completely homogeneous clusters where *all* members shared the same status - so-called "zones" (highlighted). TP = True Positive, TN True Negative, FP = False Positive, FN = False Negative, PPV = Positive Predictive Value, NPV = Negative Predictive Value. High-lighted areas on Heat Map are "zones".

Figure 3.4b. GBM patients on Avastin – tumor growth vs. no growth – using the 4 proteins with the most statistically significant p-values. The heat map in Figure 3.4a was "trimmed" by performing average linkage hierarchical clustering (supervised) on the four proteins that exhibited the most significant differences (lowest p-values) when comparing patients with tumor growth to those with no growth. Patients with high HGF and/or high TGFβ1 levels tended to exhibit tumor growth, while patients with high VEGFR2 levels and/or low TGFβ1 tended to exhibit no tumor growth.

The heat map is divided into 3 main sections consisting of samples from: 1. patients whose tumors have grown since their last evaluation (recurrence); 2. patients whose tumors have remained stable since their last evaluation (no recurrence); and 3. a mixed population of patients exhibiting either possible, slow growth or no growth. The

patient samples were then clustered with respect to the 4 proteins that were differentially expressed with the highest statistical significance (Mann-Whitney/t-test $p < 0.05$). **Figure 3.4b** shows clustering of patient samples into 3 main groups: 1. tumor growth; 2. no tumor growth; and 3. mixed population: consisting of both patients with and without tumor growth. Particularly notable is that serum levels of HGF and TGFβ1 appear to be highly upregulated in the tumor growth group as compared with the no growth group. The cytokines MIP1α and IL12 (not shown in the heatmap) are also highly upregulated in the growth group. In addition, VEGFR2 appears to be highly down-regulated, while IL2 is only somewhat downregulated, in the growth group compared with the no growth group. The alterations in cytokine levels observed in the sera of patients with growing tumors with respect to non-growing tumors may not necessarily be attributable to changes in tumor production and secretion of these cytokines. Rather, they may actually reflect changes in systemic responses to the growing tumor, such as inflammatory-associated or other immune-mediated responses.

3.4 Discussion

While antibody microarrays have been used in the past to profile cancers of the lung, liver, ovary, prostate, pancreas, colon, and bladder, this is the first study demonstrating their use for plasma profiling of glioblastoma. In this study, we have shown that by interrogating a relatively large panel of 35 plasma proteins, biomarker signatures could be straightforwardly elucidated that could differentiate GBM patients from healthy controls, and that could classify GBM patients treated with Avastin based on whether they were responsive to therapy. Furthermore, none of these proteins on its

own has been shown to be an effective biomarker for cancer diagnosis or for treatment response. Therefore, this study also reaffirmed past observations that large panels of proteins can serve as highly sensitive and specific biomarker signatures of disease, even when each component protein is a poor disease-marker on its own.

The study also showed that the predictive power of patient classification by hierarchical clustering depended on the number of differentially expressed proteins analyzed. Tests that included those proteins that were statistically significantly differentially expressed ($p < 0.05$) had greater predictive power compared with tests that additionally contained large numbers of non-discriminatory proteins or compared with tests that contained too few discriminatory proteins. The implication for future biomarker signature discovery from large numbers of proteins is that variously sized subsets of differentially expressed proteins should be evaluated to find the optimally-sized set for maximal predictive power.

In this study, the accuracy of test sample classification was also dependent on the fraction of members within the test sample's cluster that belonged to the same group (experimental vs. control). Therefore, prediction accuracy improved when evaluating only those test samples in highly biased clusters, and approached 100 % within completely homogeneous clusters. Of course, the fraction of diagnosable patients decreased as the tolerance for cluster heterogeneity was reduced. In light of this, an optimal tolerance was chosen that maximized diagnostic accuracy while minimizing the fraction of patients left out of the diagnostic evaluation. In this study, we evaluated only three tolerance settings, corresponding to exclusion of test samples in clusters that were: i. perfectly heterogeneous, ii. < 70 % homogeneous, and iii. < 100 % heterogeneous.

However, the study could potentially be reanalyzed with a larger set of tolerances to find an even better optimum. Alternatively, all patients could have been included in the diagnostic evaluation, but with the appreciation that the diagnosis of patients in certain clusters would be more accurate than in others. In theory, an accuracy score or confidence level could be calculated for grouping within any cluster. Subsequently, only those patients whose diagnoses have a predicted accuracy greater than, say, 90 % would be triaged for therapy, whereas all others would have to undergo further tests to ascertain their diagnosis. Based on our results, the diagnostic accuracy would be expected to increase with the homogeneity of a test sample's cluster, with even higher accuracies likely attainable in homogeneous clusters of larger size.

Though it might have been anticipated that plasma protein detection of brain tumors would be difficult due to the blood-brain barrier, in fact, we were able to detect differential expression of a number of factors. Many of these have been associated with systemic cancers or have been previously shown to be differentially expressed in culture media from GBM cell lines and primary cells, in the CSF fluid of GBM patients, or even in patient sera. For example, VEGF, a powerful mediator of endothelial cell proliferation and angiogenesis generally, which was found to be upregulated in GBM patients in this study, has also been shown previously to be highly secreted from GBM cell lines and primary tumors and to be expressed in the CSF fluid of glioblastoma patients[34]. VEGF is typically associated with advanced tumor stage and poor prognosis in a variety of cancers[34]. While no difference in serum expression of VEGF in the context of GBM was found by some[35], our results corroborate reports that have shown upregulated serum expression of VEGF[36]. VEGF is known to promote microvascular permeability[34], which

likely plays a role in the enhanced BBB leakiness at sites of characteristically highly neovascularized GBM tumors, thereby permitting its detection (as well as detection of a whole host of other tumor-associated proteins) in the plasma.

PDGF, which also has an important role in glioblastoma angiogenesis – particularly, in peri-endothelial cell recruitment[37] – was found to be upregulated in Avastin-treated GBM patients with growing tumors in this study. This finding is supported by past studies that have demonstrated that PDGF and its receptor are co-overexpressed in glioblastoma-derived cell lines as well as in primary GBM tumors, promoting neovascularization and tumor progression by an autocrine mechanism[38,39].

The fact that HGF levels were highly overexpressed in the sera of Avastin-treated GBM patients exhibiting tumor growth as compared to those with stable tumors confirms previous reports demonstrating that higher tumor content and CSF levels of HGF are correlated with increased tumor malignancy and poorer prognosis[40]. HGF has also been implicated in synergizing with VEGF to promote glioma angiogenesis and increased microvessel density, particularly by inducing endothelial cell proliferation[41,42]. It is also known that c-Met receptor activation by HGF enhances several oncogenic mechanisms, including cell cycle progression, proliferation, survival, migration, and invasion, and that GBM progression can be mediated by an HGF/c-Met autocrine loop[41]. Since tumors require extensive neovascularization for sustained growth, and considering the instrumental role HGF plays in GBM progression, its heightened presence in the plasma of patients with tumor growth seems sensible.

Serum IGFBP2, a binding protein that regulates the bioavailability and bioactivity of IGFs, was also found to be upregulated in this study, corroborating past reports of

elevated serum and CSF levels of IGFBP2 in patients with GBM and higher grade gliomas generally[43,44]. IGFBP2 has previously been shown to be involved in tumor growth regulation both in vitro and in vivo, and to promote glioma cell migration and invasion[45,46]. Its increased expression has therefore also been associated with increased glioma malignancy and poorer patient prognosis[43].

The ability to detect these proteins in the blood is perhaps less surprising when considering the leaky nature of newly-forming blood vessels in and around a glioblastoma tumor[20], as well as the inflammation-associated[47,48] increase in BBB permeability in the tumor's vicinity. Furthermore, not all the differentially expressed proteins detected are products of tumor cells. Many of these proteins, and particularly the cytokines, are likely secreted from inflammatory and immune cells located either in proximity to the tumor or much farther away, representing a systemic immune or inflammatory anti-tumor response. For example, GM-CSF, IP-10/CXCL-10, and IL13 were all found to be highly expressed in GBM patient plasma as compared to healthy controls. In addition, IL12, MIP1α, and TGFβ1 were all found to be highly differentially expressed in Avastin-treated GBM patients with growing tumors as compared to those with stable tumors.

Serum GM-CSF expression has previously been shown to be increased in GBM patients[36]. This is not surprising considering its important, yet conflicting, roles in promoting tumor proliferation, migration, and angiogenesis on the one hand[36,49], while on the other hand stimulating myeloproliferation in order to mount an immune/ inflammatory attack against growing tumors[48,49]. Likewise, MIP1α and its receptors have been shown to be overexpressed in GBM cells *in vitro*, and likely serve to attract

appropriate subsets of inflammatory and immune effector cells – including lymphocytes and macrophages – to the sites of tissue damage for repair[50]. However, this antitumor activity may be outweighed by an autocrine loop that promotes proliferation of the tumor cells[50]. Differential upregulation of TGFβ1 in patients with growing tumors is consistent with studies showing that tumors, such as glioblastoma, can lose their cytostatic responsiveness to this cytokine, and can instead respond to it by producing PDGF, the tumor growth promoter mentioned previously. Alternatively, tumors can overproduce and utilize TGFβ1 to suppress an antitumor host immune response and evade immune surveillance[51].

The high expression of IP-10/CXCL-10 seen in GBM patients in this study could also reflect the immune system's attempt to inhibit further tumor growth. This cytokine is secreted by monocytes, endothelial cells, and fibroblasts as a chemoattractant for recruitment of monocyte-lineage cells, T cells, and NK cells that can participate in an anti-tumor response[52]. In addition, it has previously been implicated in inhibition of angiogenesis[52], which is vital for tumor growth. Because its upregulation is induced by IFNγ, it is believed to contribute to the IFNγ-dependent anti-tumor effects of IL12[53]. This is also consistent with the upregulation of IL12 observed in this study in Avastin-treated GBM patients with tumor growth as compared to those with stable tumors. Interestingly, it also has conflicting tumor-promoting and proliferative effects on non-transformed astrocytes and cultured glioma cells, and its presence has been correlated with increased malignancy grade[54]. However, its role as a discriminatory marker in this study may be confounded by the fact that our experimental population was older than the control population, and IP-10 levels naturally increase with age, doubling between ages 40 and

$70 - 80^{55}$. Of all the analytes studied, IL13, a cytokine known to have both pro- and anti-tumor effects, showed the highest GBM patient plasma overexpression. This may be attributable to IL13 insensitivity in GBM patients as a result of GBM tumor overexpression of the "decoy" inhibitory receptor IL13Rα2[56], which may be leading to a compensatory increase in IL13 production.

Surprisingly, the levels of both CRP and MMP9 were actually decreased in GBM patient plasma as compared with healthy controls, and VEGFR2 levels were downregulated in Avastin-treated GBM patients with growing tumors as compared to those with stable tumors. Because of MMP9's documented involvement in promoting tumor invasion, as well as its anti-apoptotic and pro-angiogenic effects[57,58], its decreased plasma level in GBM patients in this study was unanticipated. Furthermore, the decrease in VEGFR2, a VEGF receptor, is unexpected since one-third of primary glioblastomas harbor amplifications in 3 receptor tyrosine kinase genes that are juxtaposed on chromosome 4: KIT, PDGFRA, and VEGFR2[59]. Furthermore, past studies have shown that VEGFR2 (and VEGFR1) is highly expressed in primary GBM tumors[60]. However, VEGFR2 downregulation could be explained by the fact that these receptors are internalized by the cell when bound by ligand. Since VEGF levels are high, a significant amount of receptor internalization could be taking place.

3.5 Future Outlook

The fact that the plasma samples used in this study could be interrogated by multiplexed antibody arrays within ELISA-like wells allowed relatively small sample volumes (< 50 μL) to be used. This suggests that these assays can in the future be

performed using blood from a fingerprick rather than the much larger quantities (milliliters) typically harvested by phlebotomy. In addition, the DNA-directed assembly of antibodies makes this platform amenable for use within microfluidics platforms, since DNA arrays can withstand the bonding temperatures required for platform assembly whereas directly-spotted antibody arrays cannot[16,33]. Therefore, a promising next step would be to integrate these arrays and antibody panels within a microfluidics-based blood separation diagnostic device. Because on-chip blood separation obviates the need for centrifugation and other blood processing steps, and due to the faster kinetics of ligand capture under conditions of fluid flow, all the assay steps within the microfluidic environment can be performed in under an hour. Consequently, a point-of-care diagnostic chip that probes for the most highly discriminatory proteins described herein for classifying patients into GBM or healthy subgroups (or for gauging treatment response) would allow patients to be diagnosed or monitored using a simple fingerprick blood test within a short time after walking into a doctor's office.

Future studies could also enlarge the microarray panel to hundreds of plasma proteins and evaluate even larger patient populations with varying grades of glioma. This could allow for higher resolution stratification of patients into diagnostic and treatment groups based on their molecular phenotypes, which could be more informative than histological grading alone. Additional studies could also assess the ability of these types of assays to classify patients as responders or non-responders shortly after initiation of treatment. Currently, using contrast-enhanced MRI imaging, it could take at least a week or more to discern whether a tumor is still growing or stable. However, it is likely that molecular changes within the tumor are occurring long before these changes manifest as

visible tumor growth and progression. Therefore, a blood test that could evaluate treatment response within hours of administration of a chemotherapeutic would allow doctors to arrive at the most effective treatment in the shortest possible time. The resulting benefits to the patient's health as well as the cost-savings could be significant.

3.6 References

1. McLendon, R.; et al. Comprehensive genomic characterization defines human glioblastoma genes and core pathways. *Nature*, **2008**, 455, 1061-1068.

2. Fauci, A. *Harrison's Principles of Internal Medicine*. New York: McGraw-Hill, 2005.

3. Deimling, A.; et al. Subsets of glioblastoma multiforme defined by molecular genetic analysis. *Brain Pathol.*, **1993**, 3, 19-26.

4. Jiang, R.; et al. Pathway alterations during glioma progression revealed by reverse phase protein lysate arrays. *Proteomics*, **2006**, 6, 2964-2971.

5. Freije, W.; et al. Gene expression profiling of gliomas strongly predicts survival. *Cancer Res.*, **2004**, 64, 6503.

6. Sreekanthreddy, P.; et al. Identification of potential serum biomarkers of glioblastoma: serum osteopontin levels correlate with poor prognosis. *Cancer Epidem. Biomar.*, **2010**, 19, 1409.

7. Huang, R. P.; Huang, R.; Fan, Y.; Lin, Y. Simultaneous detection of multiple cytokines from conditioned media and patient's sera by an antibody-based protein array system. *Anal. Biochem.*, **2001**, 294, 55-62.

8. Iwadate, Y.; et al. Molecular classification and survival prediction in human gliomas based on proteome analysis. *Cancer Res.*, **2004**, 64, 2496.

9. Schwartz, S.; Weil, R.; Johnson, M.; Toms, S.; Caprioli, R. Protein profiling in brain tumors using mass spectrometry. *Clin. Cancer Res.*, **2004**, 10, 981.

10. Mischel, P.; Cloughesy, T.; Nelson, S. DNA-microarray analysis of brain cancer: molecular classification for therapy. *Nat. Rev. Neurosci.*, **2004**, 5, 782-792.

11. Kingsmore, S. Multiplexed protein measurement: technologies and applications of protein and antibody arrays. *Nat. Rev. Drug Discovery*, **2006**, 5, 310-321.

12. Lv, L.; Liu, B. High-throughput antibody microarrays for quantitative proteomic analysis. *Expert Rev. Proteomics*, **2007**, 4, 505-513.

13. Varnum, S.; Woodbury, R.; Zangar, R. A protein microarray ELISA for screening biological fluids. *Methods in Molecular Biology -Clifton then Totowa*, **2004**, 264, 161-172.

14. Sack, R.; et al. Membrane array characterization of 80 chemokines, cytokines, and growth factors in open-and closed-eye tears: angiogenin and other defense system constituents. *Invest. Ophthalmol. Vis. Sci.*, **2005**, 46, 1228.

15. Kastenbauer, S.; Angele, B.; Sporer, B.; Pfister, H.; Koedel, U. Patterns of protein expression in infectious meningitis: a cerebrospinal fluid protein array analysis. *J. Neuroimmunol.*, **2005**, 164, 134-139.

16. Fan, R.; et al. Integrated barcode chips for rapid, multiplexed analysis of proteins in microliter quantities of blood. *Nat. Biotechnol.*, **2008**, 26, 1373-1378.

17. Hanash, S.; Pitteri, S.; Faca, V. Mining the plasma proteome for cancer biomarkers. *Nature*, **2008**, 452, 571-579.

18. Rubin, L.; Staddon, J. The cell biology of the blood-brain barrier. *Annu. Rev. Neurosci.*, **1999**, 22, 11-28.

19. Abbott, N. Inflammatory mediators and modulation of blood–brain barrier permeability. *Cell. Mol. Neurobiol.*, **2000**, 20, 131-147.

20. Kumar, V.; Abbas, A.; Fausto, N. *Robbins and Cotran Pathologic Basis of Disease.* 7th ed. Philadelphia: Saunders, 2005.

21. Leon, S.; Folkerth, R; Black, P. Microvessel density is a prognostic indicator for patients with astroglial brain tumors. *Cancer*, **1996**, 77, 362-372.

22. Kargiotis, O.; Rao, J.; Kyritsis, A. Mechanisms of angiogenesis in gliomas. *J. Neuro-Oncol.*, **2006**, 78, 281-293.
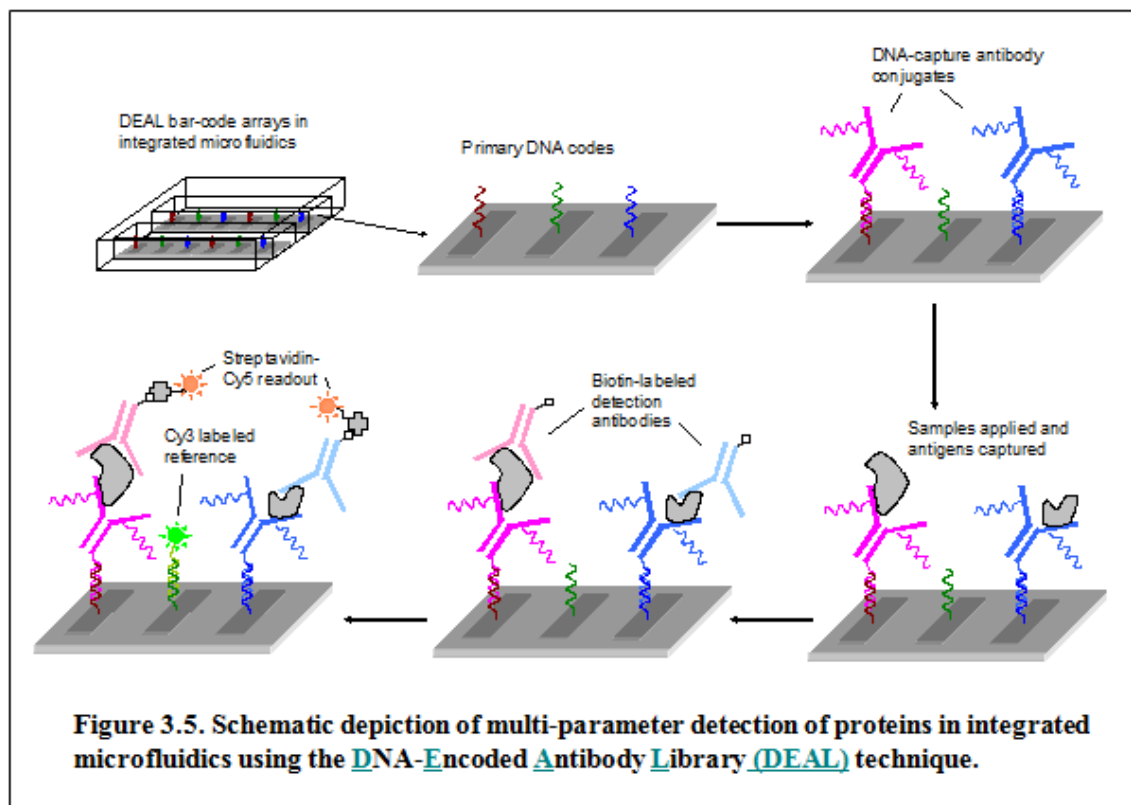
23. Schneider, S.; et al. Glioblastoma cells release factors that disrupt blood-brain barrier features. *Acta Neuropathol.*, **2004**, 107, 272-276.

24. Ludwig, J.; Weinstein, J. Biomarkers in cancer staging, prognosis and treatment selection. *Nat. Rev. Cancer*, **2005**, 5, 845-856.

25. Jiang, R.; Li, J.; Fuller, G.; Zhang, W. "Proteomic Profiling of Human Brain Tumors." *CNS Cancer*. Ed. van Meir, E. G. London: Harwood Academic Publishers, 2009. pp. 553-575.

26. Ray, S.; et al. Classification and prediction of clinical Alzheimer's diagnosis based on plasma signaling proteins. *Nat. Med.*, **2007**, 13, 1359-1362.

27. Wulfkuhle, J.; Liotta, L; Petricoin, E. Proteomic applications for the early detection of cancer. *Nat. Rev. Cancer*, **2003**, 3, 267-275.

28. Sanchez-Carbayo, M.; Socci, N.; Lozano, J.; Haab, B.; Cordon-Cardo, C. Profiling bladder cancer using targeted antibody arrays. *Am. J. Pathol.*, **2006**, 168, 93.

29. Orchekowski, R.; et al. Antibody microarray profiling reveals individual and combined serum proteins associated with pancreatic cancer. *Cancer Res.*, **2005**, 65, 11193.

30. Miller, J.; et al. Antibody microarray profiling of human prostate cancer sera: antibody screening and identification of potential biomarkers. *Proteomics*, **2003**, 3, 56-63.

31. Ellmark, P.; et al. Identification of protein expression signatures associated with Helicobacter pylori infection and gastric adenocarcinoma using recombinant antibody microarrays. *Mol. Cell. Proteomics*, **2006**, 5, 1638.

32. Wacker, R.; Schröder, H.; Niemeyer, C. Performance of antibody microarrays fabricated by either DNA-directed immobilization, direct spotting, or streptavidin-biotin attachment: a comparative study. *Anal. Biochem.*, **2004**, 330, 281-287.

33. Bailey, R. C.; Kwong, G. A.; Radu, C. G.; Witte, O. N.; Heath, J. R. DNA-encoded antibody libraries: A unified platform for multiplexed cell sorting and detection of genes and proteins. *J. Am. Chem. Soc.*, **2007**, 129, 1959-1967.

34. Hicklin, D.; Ellis, L. Role of the vascular endothelial growth factor pathway in tumor growth and angiogenesis. *J. Clin. Oncol.*, **2005**, 23, 1011.

35. Takano, S.; et al. Concentration of vascular endothelial growth factor in the serum and tumor tissue of brain tumor patients. *Cancer Res.*, **1996**, 56, 2185.

36. Rafat, N.; Beck, G.; Schulte, J.; Tuettenberg, J.; Vajkoczy, P. Circulating endothelial progenitor cells in malignant gliomas. *J. Neurosurg. Pediatrics*, **2010**, 112.

37. Guo, P.; et al. Platelet-derived growth factor-B enhances glioma angiogenesis by stimulating vascular endothelial growth factor expression in tumor endothelia and by promoting pericyte recruitment. *Am. J. Pathol.*, **2003**, 162, 1083.

38. Hermansson, M.; et al. Endothelial cell hyperplasia in human glioblastoma: coexpression of mRNA for platelet-derived growth factor (PDGF) B chain and PDGF receptor suggests autocrine growth stimulation. *P. Natl. Acad. Sci. USA*, **1988**, 85, 7748.

39. Guha, A.; Dashner, K.; McBlack, P.; Wagner, J.; Stiles, C. Expression of PDGF and PDGF receptors in human astrocytoma operation specimens supports the existence of an autocrine loop. *Int. J. Cancer*, **1995**, 60, 168-173.

40. Garcia-Navarrete, R.; Garcia, E.; Arrieta, O.; Sotelo, J. Hepatocyte growth factor in cerebrospinal fluid is associated with mortality and recurrence of glioblastoma, and could be of prognostic value. *J. Neuro-Oncol.*, **2010**, 97, 347-351.

41. Abounader, R.; Laterra, J. "HGF/c-Met Signaling and Targeted Therapeutics in Brain Tumors." *CNS Cancer*. Ed. van Meir, E. G. London: Harwood Academic Publishers, 2009. pp. 933-952.

42. Schmidt, N.; et al. Levels of vascular endothelial growth factor, hepatocyte growth factor/scatter factor and basic fibroblast growth factor in human gliomas and their relation to angiogenesis. *Int. J. Cancer*, **1999**, 84, 10-18.

43. Lin, Y.; et al. Plasma IGFBP-2 levels predict clinical outcomes of patients with high-grade gliomas. *Neuro Oncol.*, **2009**, 11, 468.

44. Hoeflich, A.; et al. Insulin-like growth factor-binding protein 2 in tumorigenesis: protector or promoter? *Cancer Res.*, **2001**, 61, 8601.

45. Dunlap, S.; et al. Insulin-like growth factor binding protein 2 promotes glioma development and progression. *P. Natl. Acad. Sci. USA*, **2007**, 104, 11736.

46. Wang, H.; et al. Insulin-like growth factor binding protein 2 enhances glioblastoma invasion by activating invasion-enhancing genes. *Cancer Res.*, **2003**, 63, 4315.

47. Fossati, G.; et al. Neutrophil infiltration into human gliomas. *Acta Neuropathol.*, **1999**, 98, 349-354.

48. Frei, K.; et al. Granulocyte-macrophage colony-stimulating factor (GM-CSF) production by glioblastoma cells. Despite the presence of inducing signals GM-CSF is not expressed in vivo. *J. Immunol.*, **1992**, 148, 3140.

49. Mueller, M.; et al. Autocrine growth regulation by granulocyte colony-stimulating factor and granulocyte macrophage colony-stimulating factor in human gliomas with tumor progression. *Am. J. Pathol.*, **1999**, 155, 1557.

50. Kouno, J.; et al. Up-regulation of CC chemokine, CCL3L1, and receptors, CCR3, CCR5 in human glioblastoma that promotes cell growth. *J. Neuro-Oncol.*, **2004**, 70, 301-307.

51. Massagué, J.; Gomis, R. The logic of TGF [beta] signaling. *FEBS Lett.*, **2006**, 580, 2811-2820.

52. Enderlin, M.; et al. TNF- and the IFN- -inducible protein 10 (IP-10/CXCL-10) delivered by parvoviral vectors act in synergy to induce antitumor effects in mouse glioblastoma. *Cancer Gene Ther.*, **2008**, 16, 149-160.

53. Phelps, C.; Korneva, E. *Cytokines and the Brain*. Amsterdam: Elsevier Science Ltd, 2008.

54. Maru, S.; et al. Chemokine production and chemokine receptor expression by human glioma cells: role of CXCL10 in tumour cell proliferation. *J. Neuroimmunol.*, **2008**, 199, 35-45.

55. Shurin, G.; et al. Dynamic alteration of soluble serum biomarkers in healthy aging. *Cytokine*, **2007**, 39, 123-129.

56. Liu, H.; et al. Interleukin-13 sensitivity and receptor phenotypes of human glial cell lines: non-neoplastic glia and low-grade astrocytoma differ from malignant glioma. *Cancer Immunol. Immun.*, **2000**, 49, 319-324.

57. Yong, V.; Power, C.; Forsyth, P.; Edwards, D. Metalloproteinases in biology and pathology of the nervous system. *Nat. Rev. Neurosci.*, **2001**, 2, 502-511.

58. Egeblad, M.; Werb, Z. New functions for the matrix metalloproteinases in cancer progression. *Nat. Rev. Cancer*, **2002**, 2, 163-176.

59. Puputti, M.; et al. Amplification of KIT, PDGFRA, VEGFR2, and EGFR in gliomas. *Mol. Cancer Res.*, **2006**, 4, 927.

60. Huang, H.; Held-Feindt, J.; Buhl, R.; Mehdorn, H.; Mentlein, R. Expression of VEGF and its receptors in different brain tumors. *Neurol. Res.*, **2005**, 27, 371-377.

3.7 Appendix A: DNA-Encoded Antibody Libraries (DEAL) Technique

Figure 3.5. Schematic depiction of multi-parameter detection of proteins in integrated microfluidics using the DNA-Encoded Antibody Library (DEAL) technique.

The advantages of DEAL are multifold. First, the fact that DNA hybridization is utilized as an assembly strategy allows for multiple proteins to be detected within the same microenvironment, since the various 1° CA antibodies for the various proteins to be detected can be each labeled with a different ssDNA oligomer (**Figure 3.5**). Second, antibodies are not particularly stable, and this makes surfaces onto which antibodies are attached unstable towards drying out, heating, etc. This means that the antibody must be attached to the surface immediately prior to use. Using DNA hybridization as an assembly strategy means that the surface can be prepared ahead of time, dried out,

heated, shipped around, etc. The instability of antibodies also makes protein assays difficult to execute within microfluidics environments, since the antibodies don't survive the microfluidics fabrication. This is, again, circumvented with the DEAL approach.

3.8 Appendix B: Patient Characteristic Tables

Table 3.1. GBM patient vs. healthy control population characteristics.

		GBM		Healthy	
		Patients	Samples	Patients	Samples
Total		46	72	47	47
Age	Median	56	56	39	39
	Mean	56	56	41	41
	Range	30-82	30-82	18-72	18-72
Gender	Male	28	48	22	22
	Female	18	24	18	18
	N/A			7	7
Treatment	No Avastin	11	14	47	47
	Avastin	24	36	0	0
	Avastin 184	2	6	0	0
	Pre-Avastin	7	14	0	0
	N/A	2	2	0	0
Recurrence	New	5	9	N/A	N/A
	1st	14	24	N/A	N/A
	2nd	5	6	N/A	N/A
	3rd	2	7	N/A	N/A
	4th	2	2	N/A	N/A
Blood Draws	1	27		47	
	2	12		0	
	3	4		0	
	4	1		0	
	5	1		0	

Table 3.2. Avastin-treated GBM patients: characteristics of patient population with and without tumor recurrence.

		Tumor Growth		No Tumor Growth	
		Patients	Samples	Patients	Samples
Total		25	52	21	51
Age	Median	56		57	
	Mean	55		54	
	Range	30-82		30-71	
Gender	Male	16	30	10	33
	Female	9	22	11	17
Treatment	Avastin	20	44	19	49
	Avastin 184	5	8	2	2
T2 Levin Score	-2	16	30	0	0
	-1	8	16	0	0
	0	3	4	21	51
	1	1	1	0	0
	2	1	1	0	0
T1C Levin Score	-2	11	22	0	0
	-1	12	16	0	0
	0	6	6	21	51
	1	5	5	0	0
	2	1	3	0	0
Recurrence	New	3	5	4	13
	1st	9	15	7	11
	2nd	3	6	2	2
	3rd	3	5	1	1
	4th	1	1	2	3
	6th	1	1	0	0
	N/A	12	18	5	5
Blood Draws	1	13		9	
	2	3		5	
	3	6		2	
	4	1		3	
	5	1		1	
	6	1		0	
	7	0		0	
	8	0		0	
	9	0		1	

3.9 Appendix C: Serum Protein Biomarker Panels and Oligonucleotide Labels

The protein panels used in the cancer-patient serum experiment (panel 1) and finger-prick blood test (panel 2), the corresponding DNA codes, and their sequences are summarized in **Table 3.3** and **Table 3.4**. These DNA oligomers were synthesized by Integrated DNA Technologies (IDT), and purified by high pressure liquid chromatography (HPLC). The quality was confirmed by mass spectrometry. The antibody vendors and catalogue numbers are listed in **Table 3.5**.

Table 3.3. List of proteins and corresponding DNA codes

DNA-code	Human Plasma Protein	Abbreviation
Panel (1)		
A/A'	Interleukin-2	IL-2
B/B'	Monocyte Chemotactic Protein 1	MCP1
C/C'	Interleukin-6	IL-6
D/D'	Granulocyte-Colony Stimulating Factor	G-CSF
E/E'	Macrophage Migration Inhibitory Factor	MIF
F/F'	Epidermal Growth Factor	EGF
G/G'	Vascular Endothelial Growth Factor	VEGF
H/H'	Platelet Derived Growth Factor	PDGF
I/I'	Transcription Growth Factor alpha	TGFα
J/J'	Interleukin-8	IL-8
K/K'	Matrix Metalloproteinase 3	MMP3
L/L'	Hepatocyte Growth Factor	HGF
M/M'	Reference (Cy3)	M'-Cy3
N/N'	Interferon-Inducible Protein 10	IP10/CXCL10
O/O'	Stromal Cell-Derived Factor 1	SDF1
P/P'	Insulin-like Growth Factor Binding Protein 2	IGFBP2
S/S'	Insulin-like Growth Factor Binding Protein 5	IGFBP5
U/U'	Macrophage Inflammatory Protein 1 alpha	MIP1α
Z/Z'	Transcription Growth Factor Beta 1	TGFβ1
AA/AA'	Chitinase 3-like 1	Ch3L1
BB/BB'	Vascular Endothelial Growth Factor Receptor 3	VEGFR3
CC/CC'	Tumor Necrosis Factor alpha	TNFα
HH/HH'	Granulocyte-macrophage colony stimulating factor	C3
II/II'	Matrix Metalloproteinase 2	MMP2
JJ/JJ'	Interleukin-10	IL-10
KK/KK'	Interleukin-1 beta	IL-1β
MM/MM'	Interleukin-12	IL-12
NN/NN'	Matrix Metalloproteinase 9	MMP9
PP/PP'	Transforming Growth Factor Beta 2	TGFβ2
QQ/QQ'	Granulocyte Macrophage Colony-Stimulating Factor	GM-CSF
RR/RR'	C-Reactive Protein	CRP
SS/SS'	Vascular Endothelial Growth Factor Receptor 2	VEGFR2
TT/TT'	Interleukin-13	IL-13
UU/UU'	Interleukin-23	IL-23
VV/VV'	Serpin E1	Serpin E1
WW/WW'	Fibrinogen	Fibrinogen

Table 3.4. List of DNA sequences used for spatial encoding of antibodies

Sequence Name	Sequence	Tm (50mM NaCl) ^{O}C
A	5'- AAA AAA AAA AAA AAT CCT GGA GCT AAG TCC GTA-3'	57.9
A'	5' NH3- AAA AAA AAA ATA CGG ACT TAG CTC CAG GAT-3'	57.2
B	5'-AAA AAA AAA AAA AGC CTC ATT GAA TCA TGC CTA -3'	57.4
B'	5' NH3AAA AAA AAA ATA GGC ATG ATT CAA TGA GGC -3'	55.9
C	5'- AAA AAA AAA AAA AGC ACT CGT CTA CTA TCG CTA -3'	57.6
C'	5' NH3-AAA AAA AAA ATA GCG ATA GTA GAC GAG TGC -3'	56.2
D	5'-AAA AAA AAA AAA AAT GGT CGA GAT GTC AGA GTA -3'	56.5
D'	5' NH3-AAA AAA AAA ATA CTC TGA CAT CTC GAC CAT -3'	55.7
E	5'-AAA AAA AAA AAA AAT GTG AAG TGG CAG TAT CTA -3'	55.7
E'	5' NH3-AAA AAA AAA ATA GAT ACT GCC ACT TCA CAT -3'	54.7
F	5'-AAA AAA AAA AAA AAT CAG GTA AGG TTC ACG GTA -3'	56.9
F'	5' NH3-AAA AAA AAA ATA CCG TGA ACC TTA CCT GAT -3'	56.1
G	5'-AAA AAA AAA AGA GTA GCC TTC CCG AGC ATT-3'	59.3
G'	5' NH3-AAA AAA AAA AAA TGC TCG GGA AGG CTA CTC-3'	58.6
H	5'-AAA AAA AAA AAT TGA CCA AAC TGC GGT GCG-3'	59.9
H'	5' NH3-AAA AAA AAA ACG CAC CGC AGT TTG GTC AAT-3'	60.8
I	5'-AAA AAA AAA ATG CCC TAT TGT TGC GTC GGA-3'	60.1
I'	5' NH3-AAA AAA AAA ATC CGA CGC AAC AAT AGG GCA-3'	60.1
J	5'-AAA AAA AAA ATC TTC TAG TTG TCG AGC AGG-3'	56.5
J'	5' NH3-AAA AAA AAA ACC TGC TCG ACA ACT AGA AGA-3'	57.5
K	5'-AAA AAA AAA ATA ATC TAA TTC TGG TCG CGG-3'	55.4
K'	5' NH3-AAA AAA AAA ACC GCG ACC AGA ATT AGA TTA-3'	56.3
L	5'-AAA AAA AAA AGT GAT TAA GTC TGC TTC GGC-3'	57.2
L'	5' NH3-AAA AAA AAA AGC CGA AGC AGA CTT AAT CAC-3'	57.2
M	5'-Cy3-AAA AAA AAA AGT CGA GGA TTC TGA ACC TGT-3'	57.6
M'	5' NH3-AAA AAA AAA AAC AGG TTC AGA ATC CTC GAC-3'	56.9
AA	5'-AAAAAAAAAAATAAGCCAGTGTGTCGTGTCT-3'	58
AA'	5'NH3-AAAAAAAAAAAGACACGACACACTGGCTTA-3'	58.1
BB	5'-AAAAAAAAAAAGTCTGATCCCATCGCGTAT-3'	57.8
BB'	5'NH3-AAAAAAAAAAAATACGCGATGGGATCAGACT-3'	57.8

CC	5'-AAAAAAAAAAGAGGTCAGTTCACGAAGCTC-3'	58.2
CC'	5'NH3-AAAAAAAAAAGAGCTTCGTGAACTGACCTC-3'	58.2
HH	5'-AAAAAAAAAAGCACTAACTGGTCTGGGTCA-3'	59.2
HH'	5'NH3-AAAAAAAAAAATGACCCAGACCAGTTAGTGC-3'	58.4
II	5'-AAA AAA AAA AGT CAG GTG TTC GCG CTC ATT -3'	60.1
II'	5'NH3-AAA AAA AAA AAA TGA GCG CGA ACA CCT GAC -3'	59.4
JJ	5'-AAA AAA AAA AGA TCG TAT GGT CCG CTC TCA -3'	58.8
JJ'	5'NH3-AAA AAA AAA ATG AGA GCG GAC CAT ACG ATC -3'	58
KK	5'-AAA AAA AAA AAC AGG TCA TCG AAC TCT CAG -3'	56.7
KK'	5'NH3-AAA AAA AAA ACT GAG AGT TCG ATG ACC TGT -3'	57.5
MM	5'-AAA AAA AAA AGG CGG CTA TTG ACG AAC TCT -3'	59.5
MM'	5'NH3-AAA AAA AAA AAG AGT TCG TCA ATA GCC GCC -3'	58.8
NN	5'-AAA AAA AAA AGC AGG GAA TTG CCG ACC ATA -3'	59.9
NN'	5'NH3-AAA AAA AAA ATA TGG TCG GCA ATT CCC TGC -3'	59.1
PP	5'-AAA AAA AAA ACG CGG CGT GTC TCA GAA TAT -3'	59.8
PP'	5'NH3-AAA AAA AAA AAT ATT CTG AGA CAC GCC GCG -3'	58.9
QQ	5'-AAA AAA AAA AAT CCG GTC TCA TCG CTG AAT -3'	58.2
QQ'	5'NH3-AAA AAA AAA AAT TCA GCG ATG AGA CCG GAT -3'	58.2
RR	5'-AAA AAA AAA AAA TGC TCA CAT CGC AGG TAC -3'	57.6
RR'	5'NH3-AAA AAA AAA AGT ACC TGC GAT GTG AGC ATT -3'	58.3
SS	5'-AAA AAA AAA AAC GCT AAT GAC GGC AGT GCA -3'	60.4
SS'	5'NH3-AAA AAA AAA ATG CAC TGC CGT CAT TAG CGT -3'	60.3
TT	5'-AAA AAA AAA AAT GTG TCC GAA CGT CGA GCT -3'	59.8
TT'	5'NH3-AAA AAA AAA AAG CTC GAC GTT CGG ACA CAT -3'	59.8
UU	5'-AAA AAA AAA AGC CGT CGG TTC AGG TCA TAT -3'	59.4
UU'	5'NH3-AAA AAA AAA AAT ATG ACC TGA ACC GAC GGC -3'	58.7
VV	5'-AAA AAA AAA AGT CGC GGG TTC TGC ACA TAT -3'	59.9
VV'	5' NH3-AAA AAA AAA AAT ATG TGC AGA ACC CGC GAC -3'	59.2

* All amine-terminated strands were linked to antibodies to form DNA-antibody conjugates using SFB/SANH coupling chemistry described by R. Bailey et al.[33] Codes AA-HH were used in the experiment examining fresh whole blood from a healthy volunteer. Codes A-M were used for the molecular analyses of cancer patient serum samples.

Table 3.5. Antibody vendors and catalogue numbers

	Company	Capture Antibody (Catalogue #)	Detection Antibody (Catalogue #)
IL2	BD	555051	555040
MCP1	eBioscience	16-7099-85	13-7096-85
IL6	eBioscience	16-7069-85	13-7068-85
G-CSF	R&D systems	MAB214	BAF214
MIF	R&D systems	MAB289	BAF289
EGF	R&D systems	MAB636	BAF236
VEGF	R&D systems	MAB293	BAF293
PDGF	R&D systems	MAB1739	BAF221
TGFa	R&D systems	AF-239-NA	BAF239
IL8	BD	554718	554716
MMP3	R&D systems	AF513	BAF513
HGF	R&D systems	MAB694	BAF294
IP10	R&D systems	MAB266	BAF266
SDF1	R&D systems	MAB350	BAF310
IGFBP2	R&D systems	MAB6741	BAF674
IGFBP5	R&D systems	MAB8751	BAF875
MIP1a	R&D systems	AF-270-NA	BAF270
TGFb1	BD	559119	559119
Ch3L1	R&D systems	DY2599	DY2599
VEGFR3	R&D systems	MAB349	BAM3492
TNFa	eBioscience	16-7348-85	13-7349-85
C3	abcam	ab17455-100	ab14232-50
MMP2	R&D systems	DY1496	DY1496
IL10	eBioscience	16-7108-85	13-7109-85
IL1b	eBioscience	16-7018-85	13-7016-85
IL12	eBioscience	14-7128-82	13-7129-85
MMP9	R&D systems	MAB9092	BAM909
TGFb2	R&D systems	DY302	DY302
GM-CSF	BD	554502	554505
CRP	R&D systems	MAB17071	BAM17072
VEGF R2	R&D systems	MAB3573	BAF357
IL13	eBioscience	16-7139-81	13-7138-81
IL23	eBioscience	14-7238-85	13-7129-85
Serpin E1	R&D systems	MAB1786	BAF1786
Fibrinogen	abcam	ab10066-250	ab14790-200

3.10 Appendix D: DNA Crosstalk Validation Assay

Figure 3.6. Test for DNA cross-hybridization. 36 ssDNA oligonucleotides (dye conjugates) were each tested separately for orthogonality against the full set of 36 surface-bound complementary strands. Red = M′-Cy5 reference. Green = Cy3-conjugated oligonucleotide. However, for **PP**, **QQ**, **UU**, and **VV**: Green = M′-Cy3 reference, Red = Cy5-conjugated oligonucleotide. Cross-hybridization was far less than the 5% cut-off for all oligonucleotides except for **I**, where the cross-hybridization level with **F** was 8% (and can be distinctly seen in the image).